RSC Advances

ROYAL SOCIETY OF CHEMISTRY

www.rsc.org/advances

Cite this: DOI: 10.1039/c0xx00000x

www.rsc.org/xxxxxx

ARTICLE TYPE

Nanoengineered CdSe quantum dots-Montmorillonite composites: An efficient photocatalyst under visible light irradiation

Rajeev C. Chikate [a,*], Brijesh S. Kadu[a] and Madhura A. Damle[b]

Received (in XXX, XXX) Xth XXXXXXXXX 20XX, Accepted Xth XXXXXXXXX 20XX

DOI: 10.1039/b000000x

In this paper, we have developed an efficient electrostatic self-assembly strategy for the synthesis of CdSe-CTAB-MMT composite that contains well-dispersed CdSe quantum dots (CdSe QD'S) within MMT structure. These nanocomposites are characterised by XRD, TEM, Raman, DRS and photoluminescence studies which indicate that 3-5 nm sized CdSe QD's are intercalated within lamellar sheets of MMT. Visible light induced photocatalytic activities of composites exhibit efficient decolourisation of 100 mg L^{-1} Indigo Carmine (IC) solution within 30 min. at 1.0 g L^{-1} catalyst loading. Such a feature may be attributed to efficient separation of photogenerated electron−hole pair, enhanced interlayer spacing (7.2 A°), higher specific surface area and better adsorption capacity of MMT. The involvement of reactive oxygen species (ROS) in the photodegradation process is ascertained by addition of selective quenchers such as NaN_3 (for singlet oxygen), benzoquinone (for $O_2^{\bullet-}$), ascorbic acid (for $OH^{\bullet}$) and KI (for h^+). It is observed that singlet oxygen and photogenerated h^+ do not contribute towards degradation; rather $O_2^{\bullet-}$ is prominent species that degrades ~74% of IC while the remaining part is oxidized by $OH^{\bullet}$. The photodegradation pathway involves desulphonation of IC followed by its oxidation to isatin, anthranilic acid, tryptanthrin and isatoic anhydride. The antibacterial studies of degraded IC solution as well as chemoinformatics studies suggest that these metabolites are non-toxic in nature. These catalysts remain active up to 6 cycles with marginal decrease in their removal capacity that can be ascribed to inhibition of photocorrosion even after successive exposure to light. Thus, nano-engineered CdSe-composites may be regarded as efficient photocatalysts that have potential applications in sustainable developments towards continuous removal of organic dyes from aqueous streams.

1. Introduction

Semiconductor photocatalysis, an environmental benign process, can address issues related to energy shortages and environmental remediation of organic pollutants.[1] However, photo-efficiency of these catalysts is restricted due to: (i) low quantum yield as a consequence of fast recombination of hole (h^+) and electron (e^-); (ii) poor absorption capacity in visible light and (iii) moderate reaction rates that severely affect the development of high throughput process.[2,3] To overcome these lacunas, two strategies are adopted: (a) shifting the photoabsorption process in visible region by doping of noble metals[4] and (b) separation of photogenerated charge carriers *via* formation of semiconducting composites.[5]

Semiconductor assisted degradation of pollutants proceeds through sequence of events that occur on the photocatalytic surface as: (a) generation of e^- and h^+ pairs through absorption of photons (b) their separation to avoid recombination process (c) oxidation of the organics by the photo-generated h^+ (d) formation of ROS like $OH^{\bullet}$, $O_2^{\bullet-}$ and H_2O_2 *via* reduction of dissolved oxygen by photogenerated e^- and (e) oxidation of organics by ROS.[6] It is envisaged that these oxidative species are primarily responsible for the degradation of dyes and these secondary metabolites are identified using chromatographic techniques to elucidate the degradation mechanism.[7-12] However, none of these reports have focused on establishing the relationship between ROS and degraded products, rather majority of them have probed formation of ROS through variety of spectroscopic techniques. For example, generation of $O_2^{\bullet-}$ and $OH^{\bullet}$ radicals is established with ESR-DMPO spin-trapping technique where low degradation activity was observed with TiO_2 based photocatalysts.[13,14] Moreover, kinetics of degradation of dyes in presence of scavenger for h^+ revealed that it predominantly influences the degradation while photogenerated e^- exhibit negligible contributions towards reductive cleavage.[15-17] Fluorescence method is also applied for the detection of $OH^{\bullet}$ with various TiO_2 powders under UV irradiation.[18] Therefore, the exact role of ROS

[a]*Nanoscience Group, Department of Chemistry, Post-graduate and Research Centre, MES Abasaheb Garware College, Karve Road, Pune-411004, India.*

bDepartment of Biotechnology, MES Abasaheb Garware College, Karve Road, Pune-411004, India

Fax: 91-20-25438165; Tel: 91-20-41038263;

E-mail: rajuchikate29@gmail.com

†Electronic Supplementary Information (ESI) available: Chemical structure of IC, Photocatalytic reactor, Kinetics, pH effect, Mass Spectra of metabolites, Antibacterial studies and Cheminformatics data of metabolites. See DOI: 10.1039/b000000x/

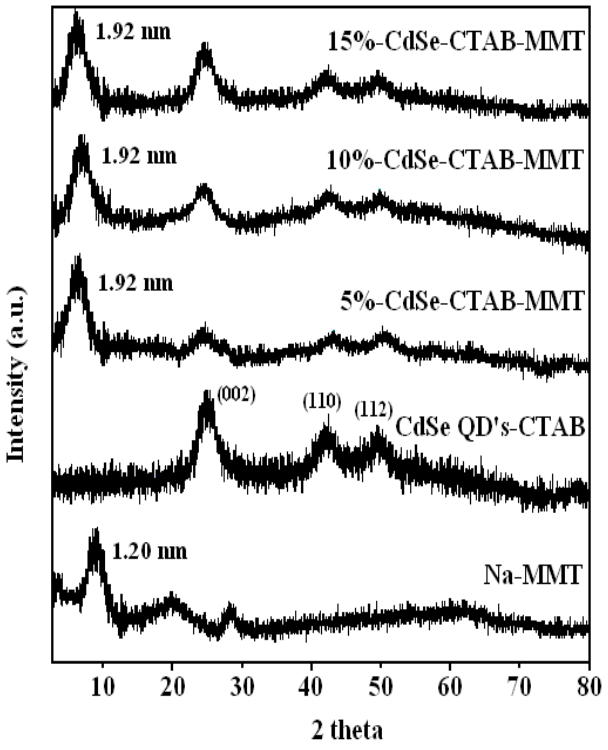

Fig. 1 X-ray diffraction patterns of CdSe-nanocomposites.

in the degradation and subsequent formation of secondary metabolites is still remained speculative.

To address this issue, we have explored two strategies: (i) separation of photogenerated e^- and h^+ pair by forming semiconductor nanocomposites and (ii) probing the role of ROS in the degradation process by monitoring the formation of secondary metabolites. To ascertain these hypotheses, CdSe-MMT nanocomposites are employed as photocatalyst for visible light driven photocatalytic degradation of IC (Supplementary data; Fig. S1). CdSe, an n-type semiconductor with band gap[19] in the range from 1.65 to 1.8 eV has received wide applications in labelling, sensors, optometric devices, solar cells and photocatalysis. Although it has extensively been employed for biological applications[20], its immobilization onto a solid support for photocatalytic applications is still remained unexplored. For this purpose, MMT is selected as a support because it possesses (i) high cation exchange capacity (119 meq/100g),[21] (ii) hydroxyl groups on the edges, (iii) beneficial Lewis and Bronsted acidity and (iv) potentiality towards formation of laminar structures through intercalation.[22, 23] This approach is beneficial for better photoabsorption followed by degradation of organic pollutants as well as for repetitive usage of photocatalysts.[24] We have also tried to establish the correlationship between ROS and the degraded products of IC *via* radical quenching experiments and proposed ROS mediated degradation pathway.

To assess the environmental implications, antibacterial activity of degraded IC solution is carried out against *E.coli*, *B.subtilis* and *S.aureus*. Since the isolation of individual metabolite is not possible at our end, their drug-like activity and related properties are evaluated with chemo-informatics softwares such as Mole Inspiration Properties Calculator (MIPC) and Molsoft to evaluate their environmental hazards.

2. Experimental

2.1. Chemicals

All chemicals were of analytical grade and used as received. IC (Hi-Media Chemicals, UK) Cadmium acetate ($Cd(OAc)_2$. $2H_2O$, Loba Chemie, UK), Selenium powder (Loba Chemie, UK), Cetyl trimethyl ammonium bromide (Sigma Aldrich); Montmorillonite K-10 (Fluka) and Sodium borohydride ($NaBH_4$, Loba Chemie, UK).

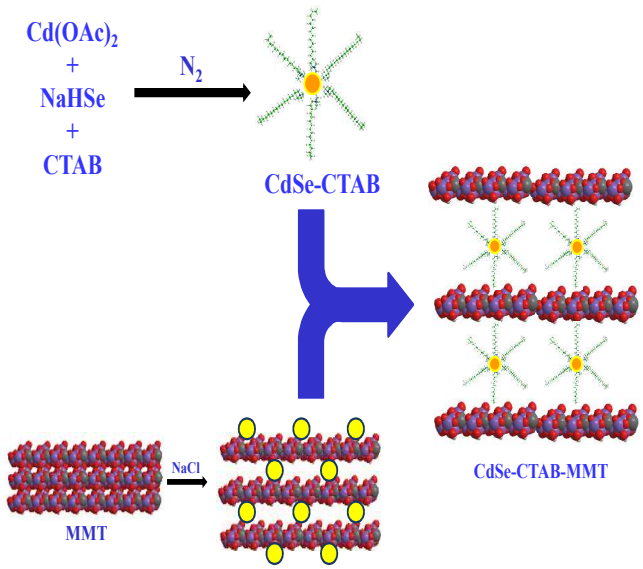

Scheme 1 Graphical illustration of the synthesis of intercalated CdSe QD's in MMT sheets

2.2. Pretreatment of MMT

MMT clay was digested with excess 1M NaCl solution for 24 h at 60°C and the solid was filtered, washed with acetone then dried at 50°C. The powder was dispersed in distilled water to prepare the colloidal suspension of clay particles and kept overnight. It was filtered, washed with distilled water and acetone and finally dried under vacuum.

2.3. Synthesis of Cadmium selenide (CdSe QD's-CTAB)

0.3 g of $NaBH_4$ in 5 mL water was added to 0.78 g Se in 5 mL water to obtain wine red coloured solution of sodium hydrogen selenide (NaHSe). In other flask, aqueous solution of cadmium acetate (1.3 g in 10 mL water) was mixed with 10 mL CTAB (0.02 M) solution. To this mixture, NaHSe solution was added drop wise with constant stirring at 40°C and the resulting mixture was kept under stirring for 1 h. Wine red coloured product was centrifuged at 3000 rpm, successively washed with methanol and then dried under vacuum.

2.4. Preparation of CdSe-CTAB–MMT nanocomposite

0.2 g of CdSe was suspended in 15 mL distilled water and the whole mixture was sonicated for 4 h. This solution was added to an aqueous suspension of 1.8 g Na-MMT in 10 mL of water and the whole mixture was stirred at 40°C for 2 h. The wine red mixture was filtered, washed successively with distilled water and finally with acetone and the product was dried under vacuum. This resulted in 10%-CdSe-CTAB-MMT composite and similar procedure was adopted for the preparation of 5% and 15% compositions.

2.5. Characterization of nanocomposites

X-ray powder diffraction (XRD) spectra were recorded on Phillips X'pert MPD X-ray diffractometer using CuKα radiation. Transmission electron microscope (TEM) images were obtained on JEOL electron microscope (model 1200X). Field emission scanning electron microscope (FE-SEM) images were obtained on Hitachi S-4800. Raman spectra were recorded on Horiba JY

Cite this: DOI: 10.1039/c0xx00000x

www.rsc.org/xxxxxx

ARTICLE TYPE

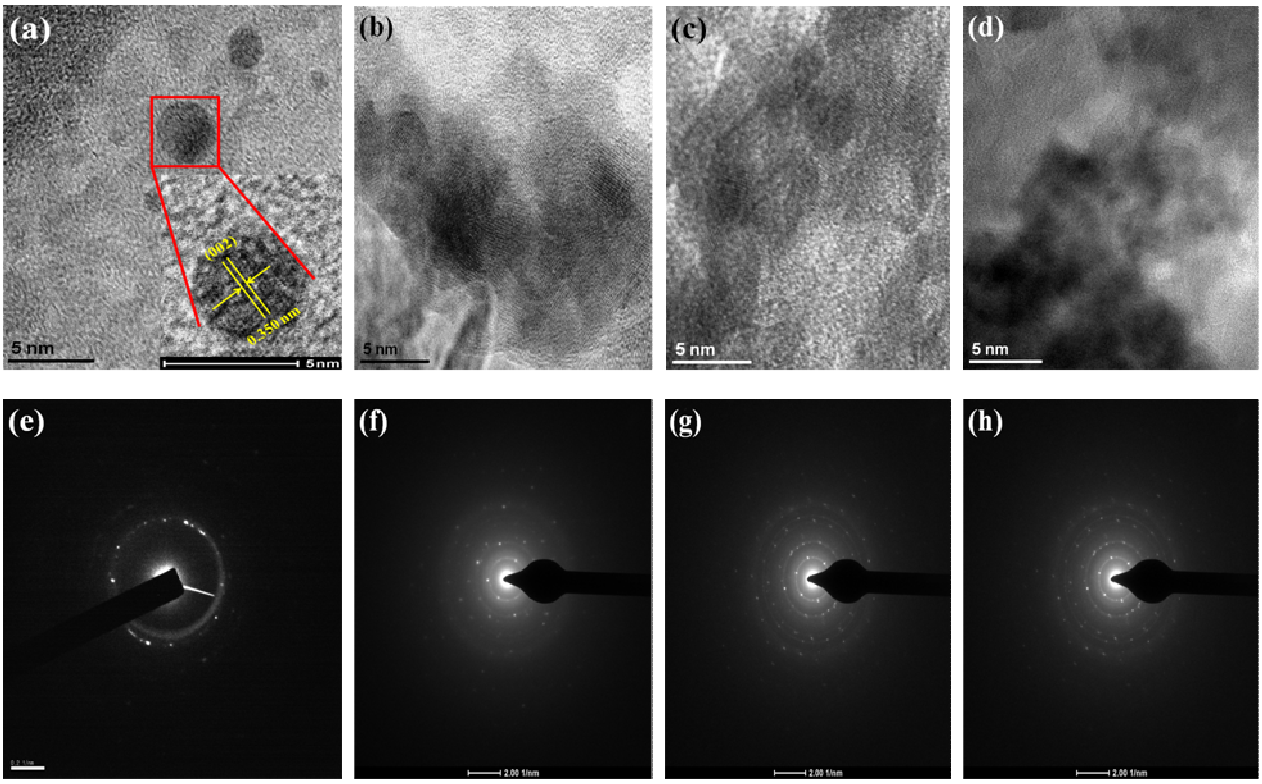

Figure 2: HR-TEM images of (a) CdSe QD's-CTAB (b) 5%-CdSe-CTAB-MMT (c) 10%-CdSe-CTAB-MMT, (d) 10%-CdSe-CTAB-MMT and SAED patterns of nanocomposites (e-f)

LabRAM HR 800 micro-Raman spectrometer operating at 17 mW and 632.8 nm excitation. Diffuse reflectance spectra of the solid samples were measured on a Shimadzu UV-VIS-NIR-3101PC scanning spectrophotometer using an integrated sphere. Photoluminescence (PL) spectra were recorded on a Hitachi F-4500 fluorescence spectrophotometer with the excitation wavelength of 450 nm. UV-VIS spectra were recorded on UV-VIS spectrophotometer (Perkin Elmer, Lambda 25). ICP-OES measurements were carried out on Optima 7000 DV ICP-OES Spectrometer (Perkin–Elmer).

2.6. Photocatalytic measurements

The photocatalytic activities of CdSe-CTAB-MMT composites were evaluated for the degradation of IC (100 mg L^{-1}) prepared in distilled water. 100 mg of the catalyst was added the 100 mL of the IC solution in a 250 mL quartz reactor (Supporting information Fig. S2) placed inside a dark box. The mixture was stirred in the dark for 30 min to establish baseline correction after adsorption of dye on catalyst. It was then irradiated with Xenon lamp (500W Xe lamp with a 420 nm cutoff filter) and 5 mL aliquots were withdrawn at certain time intervals to monitor the absorbance of supernatant at 610 nm.

2.7. Identification of Metabolite

The identification of degraded products was carried out on LC-MS (Dionex, Ultimate 3000) chromatographic system interfaced to a PE SCIEX model API3000 Triple Quadruple mass spectrometer equipped with a turbo ion spray interface. Samples were eluted at 1.5 mL min^{-1} through an Inertsil ODS 3 V column (5 µm, 150 mm X 4.6 mm) using gradient: from 0/100 (ammonium acetate 10 mM in acetonitrile/ water) to 90/10 in 25 min, which was then maintained for 6 min. The interface conditions for the positive ion mode were as follows: nebulizer gas = 8 mL min^{-1}, curtain gas = 12 mL min^{-1}, needle voltage = 4500 V at 450°C, orifice declustering potential = +10 V and focusing potential = 100 V. The flow from the HPLC-UV was split to allow 200 µL min^{-1} to enter the turbo ion spray interface.

2.8. Quenching experiments

The quenching experiments carried out with radical scavengers were as follows:

To 100 mL IC solution containing 100 mg nanocomposite, 0.2 mM of appropriate quencher was added and the entire mixture was illuminated for 30 min. using Mercury lamp in a photocatalytic reactor. The mixture was centrifuged at 3000 rpm and the supernatant was subjected for LC-MS analysis.

2.9. Reusability studies

The recycling experiments were carried out on $[IC]_{ini}$ = 100 mg L^{-1} with 1 g L^{-1} nanocomposite. After each photodegradation experiment, solution was centrifuged at 3000 rpm successively and the catalyst was carefully separated from liquid phase by a simple decantation. The recovered catalyst was successively washed with water and acetone and then used for subsequent cycles.

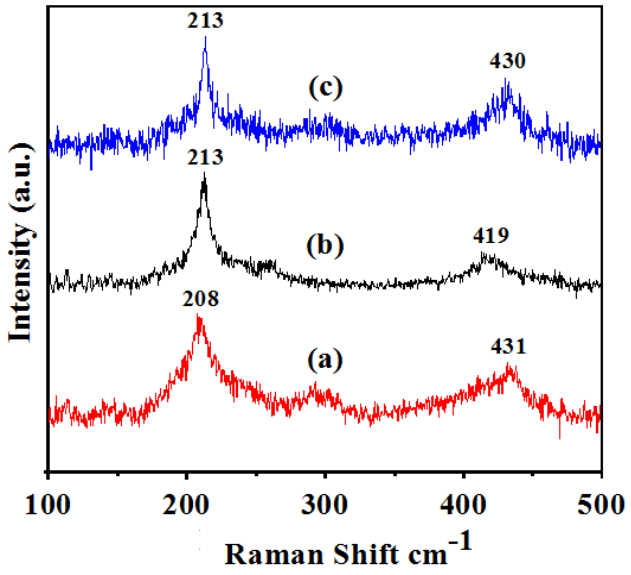

Fig. 3 Raman Spectra of (a) CdSe QD's-CTAB (b) 5%-CdSe-CTAB-MMT and (c) 10%-CdSe-CTAB-MMT

2.10. Antibacterial study

Antibacterial activity of IC and its degraded solution was evaluated with *E. coli* (NCIM-2065), *B. subtilis* (NCIM-2063) and *S. aureus* (ATCC-6538). All cultures were grown overnight at 37°C in an incubator shaker maintained at 120 rpm. The cell suspension was made from the cultures under sterile physiological saline (10^6 CFU/ml) condition. Nutrient agar plates were prepared by pour plate method using 0.1 mL of cell suspension and 6 mm sized wells were bored inside the gel. 40 µl of both IC and its degraded solution was added in the wells and the plates were incubated at 37°C for 24 hrs. Distilled water was used as the control. After 24 hrs of incubation, the zone of inhibition was measured.

3. Results and discussion

The strategy adopted for the synthesis of nanocomposites is illustrated in Scheme 1. It comprises of three processes: (i) pretreated Na-Montmorillonite exfoliates into the separate sheets when dispersed in the distilled water (ii) size quantization of CdSe due to its capping with CTAB (iii) formation of CdSe/CTAB/Clay sandwich-like adduct through self-assembly of exfoliated MMT and CTAB coated CdSe QD's *via* ion-exchange mechanism. Na^+ ions present in the interlayers of MMT undergo exchange reaction with homogeneously dispersed CdSe QD's. It results in the formation of intercalated clay structure whose basal spacing increases by ~0.7nm suggesting the laminar structure for CdSe-CTAB-MMT composite.

3.1. Characterisation of nanocomposites

X-ray diffraction patterns of CdSe QD's and its nanocomposites are shown in Fig. 1. The reflections appearing at 25.36°, 42.7° and 50.58° due to (002), (110), (112) planes correspond to Wurtzite structure[25] of CdSe (JCPDS 08-0459) while pre-treated MMT exhibits characteristic (001) peak at 7.8°. Upon composite formation between Na-MMT and CdSe-CTAB, the peak positions corresponding CdSe Wurtzite structure are retained with broadened nature. It implies that CdSe QD's are homogeneously dispersed[26] in the MMT matrix without losing its identity within the composite structure. On the other hand, from Scherer equation is found to be in the range of 2-3 nm. Thus, it may be argued that the interlayer spacing of MMT is effectively utilized for the formation of the organically modified CdSe-CTAB-MMT nanocomposites.

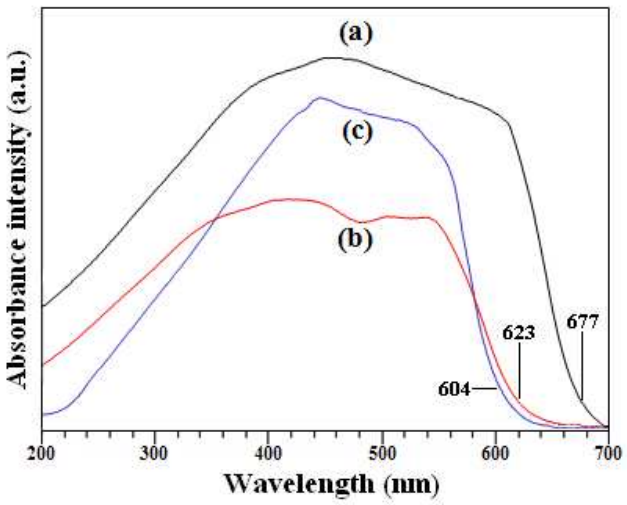

Fig. 4 DRS Spectra of (a) CdSe QD's-CTAB (b) 5%-CdSe-CTAB-MMT and (c) 10%-CdSe-CTAB-MMT

The morphology and the size of CdSe particle are investigated by TEM measurements. CdSe QD's possess spherical morphology of 3 nm size (Fig. 2a) as well as exhibited characteristic (002) plane having identical d-spacing reported for Wurtzite structure.[25] On the other hand, these QD's are uniformly distributed on the MMT matrix that results in a sheet-like structure (Fig. 2 b, c, d). Considering the enhanced interlayer spacing of MMT, it is observed that disk- or plate like CdSe QD's are properly intercalated (Supporting information Fig. S3) within the CTAB-MMT layers with particle size of about 2-3 nm. SEAD patterns of nanocomposites reveal that CdSe QD's are homogeneously dispersed within the interlayers of MMT. The specific surface area of Na-MMT, CdSe QD's, 5%- and 10%-CdSe-CTAB-MMT is found to be 34, 24.4, 68.9 and 177.0 $m^2 g^{-1}$ respectively. Higher value 10% CdSe doped MMT implies that the nanocomposite formation leads to generation nanoporous structure.

Figure 3 represents Raman spectra for CdSe QD's and its nanocomposites obtained by Lorenzian fitting methodology. A peak due to a longitudinal-optical mode of CdSe[27] is observed at 208 cm^{-1} (or 6.23 THz) for CdSe QD's while the same mode occurs at 213 cm^{-1} (or 6.38 THz) for both 5%- and 10%-CdSe-CTAB-MMT. Such a shift with broadening (FWHM = 16 cm^{-1}) for nanocomposite is caused by decrease in size as well as homogenization of CdSe crystals within MMT matrix. Similarly, 2LO photon peak for composites is also shifted towards higher energy as compared to CdSe QD's (419 cm^{-1}) which can be attributed to the relaxation of momentum conservation[28] while their broadening probably originate from negative phonon dispersion.

The absorption onsets from diffuse reflectance spectra (Fig. 4) reveal band gaps in the range 1.83-2.07 eV. It is interesting to note that there exists a blue shift for CdSe-composites as compared CdSe QD's and this observation is consistent with starch[29], oleic acid[30] and TOP/TOPO[31] capped CdSe nanocrystals. Such a feature can be attributed to ionic interaction of CdSe QD's with CTAB as well as their prohibited agglomeration due to structural rigidity of MMT layers. Thus, synergistic effect of CTAB capping and MMT results in the formation of properly dispersed CdSe QD's that generates distinct reactive sites.

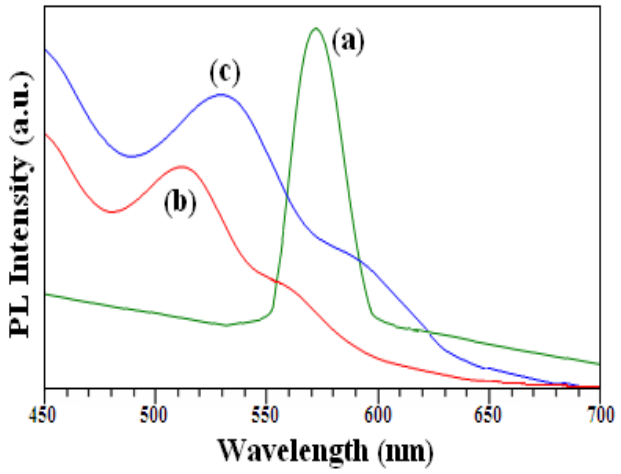

Fig. 5 Photoluminescence spectra of (a) CdSe QD's-CTAB (b) 5%-CdSe-CTAB-MMT and (c) 10%-CdSe-CTAB-MMT

The photoluminescence spectrum of CdSe QD's (Fig. 5 a) exhibit a strong emission peak at 572 nm with a full width at half-maximum (FWHM) of 26 nm and is consistent with literature reports on CdSe nanoparticles capped with thiolato-[32], chitosan-[33], PEG-[34], hexadecylamine-[35] and oleic acid[36]. On the other hand, the PL spectrum of 5% and 10% CdSe composites (Fig. 5, b-c) revealed a broad emission at 510 and 528 nm with FWHM of 56 and 64 nm respectively. Broadening in the PL spectra for composites indicates uniform shape, size, and homogeneous dispersion of CdSe QD's in the interlayer space of montmorillonite.[37, 38] The blue shift of the near band-edge emission for composites is originating from quantum confinement as well as exfoliated nature of MMT sheets.[26] It is plausible that such a feature arises due to surface defects that may lead to dissipation of emission energy and subsequent broadening of band-edge emission.[39]

3.2. Kinetics of IC degradation

The photocatalytic decolourisation of IC with CdSe QD's and their nanocomposites is carried out with 100 mg L^{-1} IC solution and 1 g L^{-1} photocatalyst. It is observed that almost 92% decolourization occurs within 30 min. (Fig. 6) for CdSe-CTAB-MMT composites while CdSe QD's exhibits lesser removal rates. These results are attributed to the pillaring of clay with CdSe QD's that lie between S–G–S layers of the clay.[38] Due to pillaring, the change in the basal space enhances the accessibility of IC towards CdSe centres that are responsible for the efficient degradation of dye in presence of light.[26] Since photocatalytic degradation of dye is a pH dependent phenomenon, effect of pH on removal capacity in the pH range of 1 - 8 is carried out on 10%-CdSe-CTAB-MMT composite. Higher removal capacity at pH 7 (Supplementary data; Fig. S4) suggests that there is deactivation of photocatalyst surface under acidic medium. Thus, further investigations are carried out with this photocatalyst at pH 7 for elucidating the degradation mechanism as well as biological screening of metabolites generated after degradation of IC molecule.

3.3. Effect of reactive oxygen species (ROS) on degradation pathway

It is well established that dissolved oxygen (D.O.) in water is the primary source for degradation of organic pollutants.[40] In order to ascertain this fact, the degradation of IC carried out in aqueous and N_2 purged (1 h) solutions (Fig. 7, inset) which suggests that only 10% of dye is decolorized under anaerobic condition as compared to ~ 90% in presence of D.O.[41] Such a small amount of

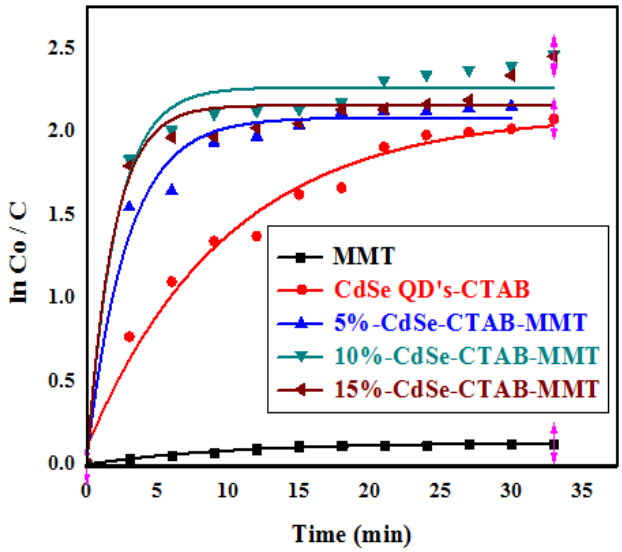

Fig. 6 Time profile of IC decolourisation by CdSe QD's-CTAB and CdSe-CTAB-MMT nanocomposites: {$[IC]_{ini}$ =100 mg L^{-1}; [Nanocomposite] = 1 g L^{-1}, at 25°C}

decolorization for N_2 purged sample may be occurring due to either adsorbed oxygen or hydroxyl groups present on photocatalytic surface.[42] However, these findings do not demonstrate the type of oxygen species responsible for oxidative cleavage of dye molecule. To substantiate this hypothesis, various scavengers such as NaN_3 (for singlet oxygen),[43] 1,4-benzoquinone (BQ; for $O_2^{\bullet-}$)[44] and ascorbic acid (AA; for $OH^{\bullet}$ radical)[45] are added to IC solution before it is irradiated with visible light. It is reported that h^+ are also responsible for oxidation of organic pollutants.[46] This aspect is evaluated by addition KI, a hole quencher, as it would hinder electron-hole recombination process as well as assist in predicting the ease at which the formation of ROS takes place through reduction of dissolved oxygen. Fig. 7 illustrates decolourisation curves for IC without and with addition of 0.02 M quenchers (b-e). It is interesting to note that quenching of h^+ and singlet oxygen does not affect degradation as the nature of graphs is almost similar to non-quenched solution. Such a feature illustrates that electron-hole recombination process is hindered due to presence of MMT layers that dissipate photogenerated electrons and subsequently facilitates the reduction of adsorbed oxygen on catalytic surface. However, when $O_2^{\bullet-}$ and $OH^{\bullet}$ radicals are scavenged, only 20% decolourisation is observed indicating that these two radicals are indeed responsible for oxidative cleavage of IC molecule.

To further corroborate the role of $O_2^{\bullet-}$ and $OH^{\bullet}$ radicals in the formation of secondary metabolites, HPLC analysis is carried out on decolorized IC solution obtained either with or without addition of quenchers (Supplementary data; Fig. S5). Chromatogram of non-quenched solution (Supplementary data; Fig. S5a) reveals that five metabolites are formed whose molecular masses are identified from MS analyses (Supplementary data; Fig. S6). Isatin (I) is found to be major degradation product (43%) followed by isatoic anhydride (III, 21%), tryptanthrin (II, 11%) and anthranilic acid (II, 10%) with formation of small amount of Indigo blue (IB, 7%). Formation these metabolites (Scheme 2) can be explained as: (i) desulphonation of IC to IB (ii) reductive cleavage of double bond resulting into isatin (I) and anthranilic acid (II) and (iii) their

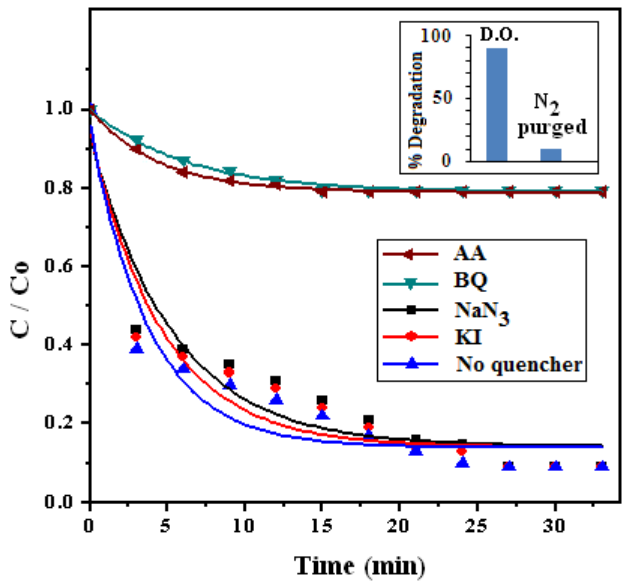

Fig. 7 Variation of normalized concentration of IC in solution in the presence of 2 mM of AA, BQ, NaN_3, and KI. Inset: Degradation rate of air equilibrated and N_2 purged condition. $\{[IC]_{ini}$ =100 mg L^{-1}; [10%-CdSe-CTAB-MMT] = 1 g L^{-1}, 25°C}

cyclisation to isatoic anhydride (III) and tryptanthrin (IV) through oxidative cleavage.[47]

On the other hand, LC-MS analysis of BQ and AA treated IC solution results in the formation of ~90% of IB through desulphonation of IC that primarily occurs in absence of ROS. It is plausible that positively charged CdSe-CTAB-MMT surface along with visible light is responsible for this step. IV is formed when $O_2^{\bullet-}$ is quenched by addition of BQ (Supplementary data; Fig. S5b) while isatin (I) and its anhydride (II) are generated after scavenging of $OH^{\bullet}$ by AA (Supplementary data; Fig. S5c). Small amount of IV is also obtained through condensation of anthranilic acid (II) and isatin (I)[48] that are formed due to oxidation of IB. It also suggests that ROS are indeed required for complete oxidation of IC; a feature already been observed for variety of photoredox processes. Conversely, quenching of $OH^{\bullet}$ leads to formation of partially oxidized metabolites I and III which suggests that $O_2^{\bullet-}$ radical initiates oxidative cleavage of IB across central double bond. The formation of significant amount of $O_2^{\bullet-}$ radical is possibly favoured due to either hindered electron-hole recombination process or photo-excitation of IC molecule. This hypothesis is further corroborated with addition of KI (h^+ quencher) where it is observed that quenching of h^+ has no effect on degradation process (Fig. 7). It suggests that photoelectrons generated from composites as well as IB is absorbed by dissolved oxygen and it is estimated that ~64% of $O_2^{\bullet-}$ are formed during the photocatalytic process. It is estimated from the amounts of different metabolites formed due to the reaction between IC and this radical (Scheme 2). However, for complete oxidation of IB to II, strong oxidizing agent such as $OH^{\bullet}$ is essential as it is only formed under aerobic condition (Supplementary data; Fig. S5a). Therefore, it may be argued that $O_2^{\bullet-}$ radical is the most prominent ROS species[49] responsible for ~ 64% degradation with further cleavage occurring in presence of $OH^{\bullet}$ radicals. Thus, quenching experiments clearly demonstrate that $O_2^{\bullet-}$ and $OH^{\bullet}$ radicals are reactive species involved in the oxidative degradation IC to oxygenated metabolites. To summarize, visible light assisted photocatalytic degradation of IC occurs through (a) desulphonation of IC to IB (b) partial oxidation with $O_2^{\bullet-}$ radical

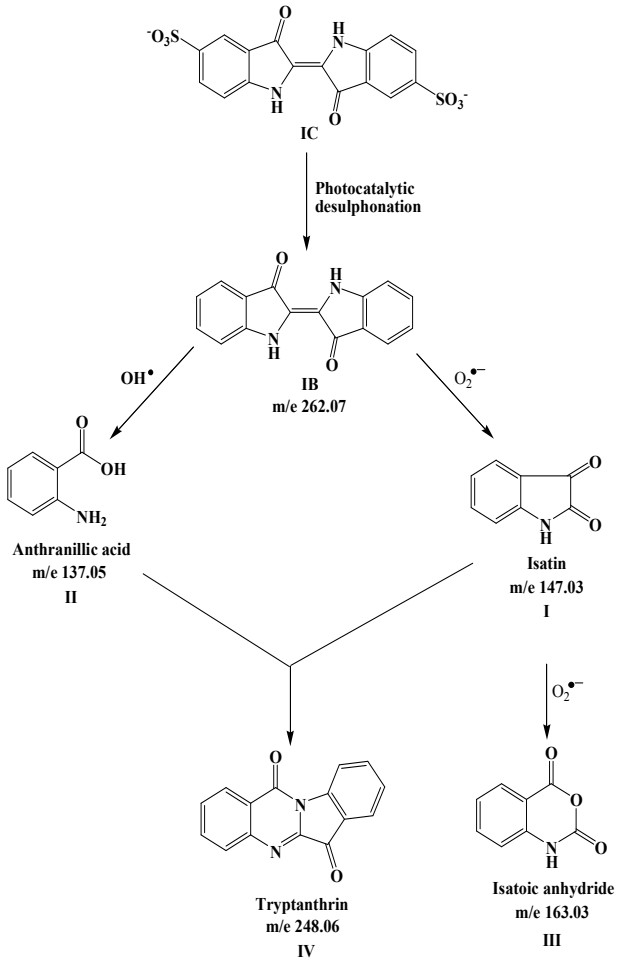

Scheme 2 Proposed degradation mechanism of IC in presence of D.O. using 10%-CdSe-CTAB-MMT

forming isatin and its anhydride and (c) generation of anthranilic acid through $OH^{\bullet}$ radical.

3.4. Reusability studies

The effectiveness of a photocatalyst is considered to be based on how it remains active during continuous illumination of light because it is quite likely that it may loose its catalytic activity due to photocorrosion. To assess this aspect, recycling experiments are carried out on recovered photocatalyst with 100 mg L^{-1} IC solution with 1 g L^{-1} photocatalyst (Fig. 8). The retention of photocatalytic efficiency during 6 cycles implies that composite surface hasn't undergone photocorrosion due to successive exposure to visible light. XRD and TEM analyses of recovered photocatalyst after 6th cycle (Supplementary Data; Fig. S7) suggest that there exist negligible structural changes as well as the morphology of composite is also retained even after its repetitive usage. Interestingly, when these results are compared with different photocatalysts[50-54] employed for IC degradation (Table 1), it is observed that 10%-CdSe-CTAB-MMT composite decolorizes IC at substantially lesser time even at higher concentration of dye reflecting its significantly higher photocatalytic efficiency. Moreover, our composite possess excellent removal efficiency with almost 520 ppm of IC is successfully removed within 3 h. Since cadmium and selenium both being toxic, it is imperative to estimate the leaching of these two species during photocatalytic experiment. It is monitored with ICP-OES measurements of supernatant obtained after 6th cycle of successive usage of 10%-CdSe-CTAB-MMT and the

Cite this: DOI: 10.1039/c0xx00000x

www.rsc.org/xxxxxx

ARTICLE TYPE

Table 1: Comparison of photocatalytic decolourisation efficiency of different photocatalysts towards Indigo carmine

Photocatalyst	Dosage ($g\ L^{-1}$)	Dye Conc. ($mg\ L^{-1}$)	Decolourisation Time (min)	% Decolourisation	Ref.
Nb_2O_5	1.0	4.66	90	100	50
Fe, N co-doped TiO_2	2.0	20	180	89	51
Ag/graphene oxide	1.0	10	420	41	52
TiO_2 on SiC	1.0	20	30	100	53
$CeAlO_3$	1.0	100	90	100	54
10%-CdSe-CTAB-MMT	1.0	100	12	92	Present work

amounts are found to be 2.9 and 4.5 ppb for cadmium and selenium respectively.

Thus, it may be argued that designing of such tailored made functional nanomaterials may be regarded as viable strategy towards the development of sustainable photocatalytic process that may possess potential applications towards continuous removal of organic pollutants from aqueous medium.

3.5. Environmental implications

Other implication of this strategy is also focused on whether the secondary metabolites that are generated during the photodegradation of a toxic dye[55] possess any environmental hazards. Two strategies are envisaged to address this issue; (i) isolation of individual metabolites through prep-HPLC and evaluate their individual toxicities and (ii) antimicrobial activity of degraded solution as a whole. However, former studies are not possible at our end while the latter approach would result in combined toxicity and not due to individual metabolite.

Antibacterial activity of IC and its degraded solution is carried out against three bacterial strains viz. *E.coli, S.aureus* and *B.subtilis* (Supplementary Data; Fig. S8). IC exhibits 6-8 mm zone of inhibition at 100 ppm; even at lower concentration (10 ppm), there exists inhibition of growth implying that IC is indeed toxic in nature. However, when 100 ppm degraded solution is exposed to these strains, there is absence of zone of inhibition suggesting that none of the five metabolites possess antibacterial activity. To corroborate this observation, we have employed chemoinformatics software commonly used for predicting drug-like activity for variety of organic molecules. After careful literature search, it is noticed that Molinspiration Property Calculator (MIPC)[56] is routinely employed for such a purpose. Employing this tool, the simulated molecular properties such as percentage of absorption, molecular polar surface area (PSA), logP, number of rotatable bonds, number of hydrogen bond donor and accepter atoms of Lipinski's rule of five are evaluated for metabolites I-IV (Supplementary Data; Table T1).

Hydrogen bond acceptor (HBA) and donor (HBD) capacities of functional groups indeed play crucial role in identifying its interaction with potential receptors that favour hydrogen bonding. It can be seen from these two parameters that number of hydrogen bond acceptor (≤ 10) and hydrogen bond donor (≤ 5) sites for I – IV obey Lipinski's rule of five implying that they possess good absorption or membrane permeability. Moreover for compounds I and II, these values are ≤ 3 indicating their drug like character. Lipophilicity (logP) is another factor that governs the passive membrane partitioning as well as influencing permeability of molecule for its subsequent absorption. This value is significantly lower for all the metabolites (0.73 – 2.90) that augurs well for their substantial lipophilicity. Generally, it is observed that higher molecular weight compounds have adverse effects on interactions with receptors and/or DNA. Such an unfavourable situation is not observed for I-IV that also corroborates with Lipinski's rule of five. Molecular polar surface area (PSA) predicts the transport property of compound and is inversely proportional to %ABS. All the metabolites have maximum absorption (> 85%) owing to their small polar surface areas. The drug-likeness model score, computed for secondary metabolites using Molsoft server suggests that tryptanthrin (IV) is the only metabolite that posses drug like properties. Thus, it may be argued that photodegradation process evaluated in the present work may be regarded as eco-friendly that does not possess any threat or hazards to environment.

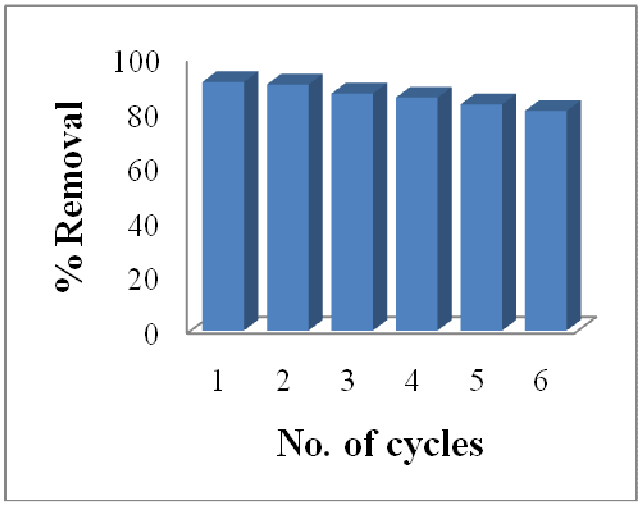

Fig. 8 Recycling efficiency of 10%-CdSe-CTAB-MMT towards removal of IC

Conclusions

Intercalated CdSe-CTAB-MMT nanocomposites with uniform dispersion of CdSe QD's are fabricated by a facile self-assembly approach that significantly enhances visible light induced photocatalytic degradation of IC. The lamellar structure of composites also hinders recombination of photogenerated electrons and holes corroborated with addition of KI; an h^+ quencher, while electrons are subsequently utilised for the formation reduced oxygen species. It is observed that $O_2^{\bullet-}$ radical is the prominent species that photodegrades IC to the tune of ~ 74% while remaining part is oxidised via $OH^{\bullet}$ radicals. The plausible degradation pathway involves desulphonation followed by oxidative cyclization and complete oxidation of IC generating anthranilic acid. Moreover, these nanocomposites are recycled without sacrificing their photocatalytic activity implying that they can be effective towards continuous removal of dyes. The degraded metabolites are found to non-toxic with negligible leaching of cadmium and selenium during photochemical process even after repetitive usage of photocatalysts. Thus, such a simple, tailored made and nanoengineered synthetic strategy can be extended for the fabrication of superior visible-light-driven photocatalysts that are robust and low-cost for diverse photochemical applications in an eco-friendly manner.

Acknowledgements

Authors are thankful to Dr. A. D. Natu, Head, Dept. of Chemistry and Dr. S.G. Gupta, Principal, A. G. College, for constant encouragement and support. DST, New Delhi is acknowledged for providing FIST grant.

References:

1 M. Yin, Z. Li, J. Kou and Z. Zou, *Environ. Sci. Technol.,* 2009, **43**, 8361-8366.
2 R. Asahi, T. Morikawa, T. Ohwaki, K. Aoki and Y. Taga, *Science,* 2001, **293**, 269-271.
3 Z. Zou, J. Ye, K. Sayama and H. Arakawa, *Nature,* 2001, **414**, 625-627.
4 M. Alonso, F. Fresno, S. Suarez and J. Coronado, *Energy Environ. Sci.,* 2009, **2**, 1231-1257.
5 D. Yang, H. Liu, Z. Zheng, Y. Yuan, J. Zhao, E. Waclawik, W. Ke and H. Zhu, *J. Am. Chem. Soc.,* 2009, **131**, 17885-17893.
6 J. Tang, Z. Zou and J. Ye, *Angew. Chem. Int. Ed.,* 2004, **43**, 4463-4466.
7 Y. Lin, D. Li, J. Hu, G. Xiao, J. Wang, W. Li and X. Fu, *J. Phys. Chem. C,* 2012, **116**, 5764-5772**.**
8 C. Chen and C. Lu, *J. Phys. Chem. C,* 2007, **111***,* 13922-13932.
9 G. Liu, X. Li, J. Zhao, H. Hidaka and N. Serpone, *Environ. Sci. Technol.,* 2000, **34**, 3982-3990.
10 C. Chen, H. Fan and J. Jan, *J. Phys. Chem. C,* 2008, **112***,* 11962-11972.
11 T. Luo, Z. Ai and L. Zhang, *J. Phys. Chem. C,* 2008, **112***,* 8675-8681.
12 S. Singh, V. Srivastava and I. Mall, *J. Phys. Chem. C,* 2013, **117**, 15229–15240.
13 S. Ribbens, I. Caretti, E. Beyers, S. Zamani, E. Vinck, S. Doorslaer and P. Cool, *J. Phys. Chem. C,* 2011, **115**, 2302-2313.
14 Y. Hou, X. Li, Q. Zhao, G. Chen and C. Raston, *Environ. Sci. Technol.,* 2012, **46**, 4042-4050.
15 X. Doorslaer, P. Heynderickx, K. Demeestere, K. Debevere, H. Langenhove and J. Dewulf, *Appl. Catal. B: Environ.,* 2012, **111-112**, 150-156.
16 L. Martinez, J. Faria, J. Rodriguez, C. Rodriguez and A. Silva, *Appl. Catal. B: Environ.,* 2012, **113-114**, 221-227.
17 W. Wang, L. Zhang, T. An, G. Li, H. Yip and P. Wong, *Appl. Catal. B: Environ.,* 2011, **108-109**, 108-116.
18 J. Zhang and Y. Nosaka, *J. Phys. Chem. C,* 2013, **117**, 1383-1391.
19 M. Kotkata, A. Masoud, M. Mohamed and E. Mahmoud, *Physica E,* 2009, **41**, 640-645.
20 W. Chan and S. Nie, *Science,* 1998, **281**, 2016-2018.
21 H. Koyuncu, *Appl. Clay Sci.,* 2008, **38**, 279-287.
22 Z. Qian, G. Hu, S. Zhang and M. Yang, *Physica B,* 2008, **403**, 3231-3238.
23 B. Hu and H. Luo, *Appl. Surf. Sci.,* 2010, **257**, 769-775.
24 B. Kadu, Y. Sathe, A. Ingle, R. Chikate, K. Patil and C. Rode, *Appl. Catal. B: Environ.,* 2011, **104**, 404-414.
25 X. Duan, X. Liu, Q. Chen, H. Li, J. Li, X. Hu, Y. Li, J. Ma and W. Zheng, *Dalton Trans.,* 2011, **40**, 1924-1928.
26 A. Ontam, N. Khaorapapong and M. Ogawa, *J. Colloid Interf. Sci.,* 2011, **357**, 554-557.
27 F. Widulle, S. Kramp, N. Pyka, A. Gobel, T. Ruf, A. Debernardi, R. Lauck, M. Cardona, *Physica B,* 1999, **263**, 448-451.
28 I. Campbell and P. Fauchet, *Solid State Commun.,* 1986, **58**, 739-741.
29 J. Li, C. Ren, X. Liu, Z. Hu and D. Xue, *Mater. Sci. Eng. A,* 2007, **458**, 319-322.
30 D. Ayele, H. Chen, W. Su, C. Pan, L. Chen, H. Chou, J. Cheng, B. Hwang and J. Lee, *Chem. Eur. J.,* 2011, **17**, 5737-5744.
31 Robel , M. Kuno and P. Kamat, *J. Am. Chem. Soc.,* 2007, **129**, 4136-4137.
32 W. Mahmoud and S. Yaghmour, *Optical Mater.,* 2013, **35**, 652-656.
33 T. Wang, S. Zhang, C. Mao, J. Song, H. Niu, B. Jin and Y. Tian, *Biosens. Bioelectron.,* 2012, **31**, 369-375.
34 Y. Sun, B. Zhou, Yi Lin, Wei Wang, K. Fernando, P. Pathak, M. Meziani, B. Harruff, X. Wang, H. Wang, P. Luo, H. Yang, M. Kose, B. Chen, L. Veca and S. Xie, *J. Am. Chem. Soc.,* 2006, **128**, 7756-7757.
35 S. Kim and H. Yang, *Current Appl. Phys.,* 2011, **11**, 1056-1059.
36 S. Bera, S. Singh and S. Ray, *J. Solid State Chem.,* **2012**, *189*, 75-79.
37 Y. Fukushima, *Clay and Clay Minerals,* 1984, **32**, 320-326.
38 S. Hur, T. Kim, S. Hwang, S. Hwang, J. Yang and J. Choy, *J. Phys. Chem. B.,* 2006, **110**, 1599-1604.
39 M. Vibin, R. Vinayakan, A. John, C. Rejiya, V. Raji and A. Abraham, *J. Colloid Interf. Sci.* 2011, **357**, 366-371.
40 P. Kamat, *Chem. Rev.,* 1993, **93**, 267-300.
41 P. Novotna, J. Boon, J. Horst and V. Pacakova, *Color. Technol.,* 2003, **119**, 121-127.
42 P. Ji, J. Zhang, F. Chen and M. Anpo, *Appl. Catal. B: Environ.,* 2009, **85**, 148-154.
43 C. Schweitzer and R. Schmidt, *Chem. Rev.,* 2003, **103**, 1685-1758
44 J. Bandara and J. Kiwi, *New J. Chem.,* 1999, **23**, 717-724.
45 A. Bokare, R. Chikate, C. Rode and K. Paknikar, *Environ. Sci. Technol.,* 2007, **41**, 7437-7443.
46 C. Chen, W. Ma and J. Zhao, *Chem. Soc. Rev.,* 2010, **39**, 4206-4219.
47 M. Sousa, C. Miguel, I. Rodrigues, A. Parola, F. Pina, J. Melo and M. Melo, *Photochem. Photobiol. Sci.,* 2008, **7**, 1353-1359.
48 A. Muruganandam and S. Bhattacharya, *Ind. J. Chem.,* 2000, **39B**, 125-131.
49 C. Guo, J. Xu, S. Wang, Y. Zhang, Y. He and X. Li, *Catal. Sci. Technol.,* 2013, **3**, 1603-1611.
50 A. Prado, L. Bolzon, C. Pedroso, A. Moura, L. Costa, *Appl. Catal. B: Environ.*, 2008, **82**, 219–224.
51 T. Kim, V. González, G. Gyawali, S. Cho, T. Sekino, S. Lee, *Cat. Today*, 2013, **212**, 75-80.
52 R. Orozco, H. Rosu, S. Lee, V. Gonzalez, J. Hazard. Mater., 2013, **263P**, 52-60.
53 C. Solis, I. Ramírez, E. Moctezuma, L. Martínez, J. Hazard. Mater., 2012, **217-218**, 194- 199.
54 P. Deshpande, S. Aruna, G. Madras, Clean – Soil, Air, Water 2011, **39**, 259-264.
55 T. Guaraldo, T. Zanoni, S. Torresi, V. Goncales, G. Zocolo, D. Oliveira and M. Zanoni, *Chemosphere,* 2013, **91**, 586-593.
56 S. Alegaon, K. Alagawadi, P. Sonkusare, S. Chaudhary, D. Dadwe and A. Shah, *Bioorg. Med. Chem. Lett.,* 2012, 22, 1917-1921.